Focal Dorsal Hippocampal Nav1.1 Knock Down Alters Place Cell Temporal Coordination and Spatial Behavior

Sophie Sakkaki, Sylvain Barriere, Alex Bender, Rod Scott, Pierre-Pascal Lenck-Santini

Cerebral Cortex, September 2020;30: 5049–5066

doi: 10.1093/cercor/bhaa101
Advance Access Publication Date: 7 May 2020
Original Article

ORIGINAL ARTICLE

Focal Dorsal Hippocampal Nav1.1 Knock Down Alters Place Cell Temporal Coordination and Spatial Behavior

Sophie Sakkaki[1,2], Sylvain Barrière[1], Alex C. Bender[3], Rod C Scott[1,5,6] and Pierre-Pascal Lenck-Santini[1,4]

[1]Department of Neurological Sciences, Larner College of Medicine, University of Vermont, Burlington, VT 05405, USA, [2]IGF, Université Montpellier, CNRS, INSERM, Montpellier 34094, France, [3]Dartmouth Geisel School of Medicine, Hanover, NH 03755 ,USA, [4]INMED, INSERM, Aix-Marseille Univ, Marseille, France, [5]UCL Institute of Child Health, 30 Guilford Street, London WC1N 1EH, UK and [6]Department of Neurology, Great Ormond Street Hospital NHS Trust, London WC1N 3JH, UK

Address correspondence to Sophie Sakkaki, Institute of Functional Genomic, Université Montpellier, CNRS, INSERM. 141, rue de la Cardonille, 34094 Montpellier cedex 05, France. Email: sophie.sakkaki@igf.cnrs.fr

Abstract

Alterations in the voltage-gated sodium channel Nav.1.1 are implicated in various neurological disorders, including epilepsy, Alzheimer's disease, and autism spectrum disorders. Previous studies suggest that the reduction of Nav1.1 expression leads to a decrease of fast spiking activity in inhibitory neurons. Because interneurons (INs) play a critical role in the temporal organization of neuronal discharge, we hypothesize that Nav1.1 dysfunction will negatively impact neuronal coordination in vivo. Using shRNA interference, we induced a focal Nav1.1 knock-down (KD) in the dorsal region of the right hippocampus of adult rats. Focal, unilateral Nav1.1 KD decreases the performance in a spatial novelty recognition task and the firing rate in INs, but not in pyramidal cells. It reduced theta/gamma coupling of hippocampal oscillations and induced a shift in pyramidal cell theta phase preference. Nav1.1 KD degraded spatial accuracy and temporal coding properties of place cells, such as theta phase precession and compression of ongoing sequences. Aken together, these data demonstrate that a deficit in Nav1.1 alters the temporal coordination of neuronal firing in CA1 and impairs behaviors that rely on the integrity of this network. They highlight the potential contribution of local inhibition in neuronal coordination and its impact on behavior in pathological conditions.

Key words: CA1, Nav1.1, place cell, SC1NA, theta

Introduction

Information processing in the nervous system depends on the temporal coordination of neural activity within brain networks (Buzsáki 2010). Such coordination is revealed by oscillatory activity in local field potentials (LFP) and is dependent upon the dynamic organization of activity within neuronal microcircuits, where each cell type acts via specific electrophysiological and connectivity principles (Barthó et al. 2004; Klausberger and Somogyi 2008). Therefore, alterations in the fundamental properties of specific cell types should have consequences on network function, leading to cognitive dysfunction (Robbe and Buzsáki 2009). While this notion is emerging as a mechanism

for neuropsychiatric disorders (Uhlhaas and Singer 2010; Fenton 2015), there is still little experimental evidence supporting it.

In epilepsy syndromes, cognitive, attentional, and behavioral deficits that define psychiatric disorders are overrepresented. In addition, seizures and/or epileptiform abnormalities are frequently observed in psychiatric disorders, suggesting that common mechanisms may be at play between these syndromes. The identification of common underlying genetic etiologies or similar cellular mechanisms in models of epilepsy and neuropsychiatric disorders has helped to highlight some of the shared mechanisms.

For example, mutations in the SCN1A gene, encoding the Nav1.1 voltage-gated sodium channel, have frequently been associated with epilepsy syndromes, such as Dravet syndrome (DS) (Catterall et al. 2010), characterized by seizures, cognitive impairment, learning disability, and autistic features. Other neurological disorders, including anxiety, autism spectrum disorders (ASD), and Alzheimer disease (AD), have also been associated with Nav1.1 dysfunction (Verret et al. 2012; D'Gama et al. 2015). Finally, Nav1.1 activators are being proposed as potential treatments for schizophrenia and AD (Jensen et al. 2014). In the context of epilepsy, growing evidence suggests that *SCN1A* mutations play a direct role in cognitive impairments, independently of seizures (Mahoney et al. 2009; Bender et al. 2013; Nabbout et al. 2013; Villeneuve et al. 2014; Passamonti et al. 2015).

A link between Nav1.1 alterations and cognitive/behavioral impairment may be provided by the fact that, although Nav1.1 is expressed in most neuronal cell types, its loss appears to more selectively impact GABAergic neurons. For instance, Bender et al. (Bender et al. 2013, 2016) showed that the Nav1.1 loss of function locally induced in the medial septum disrupted fast-firing neurons activity, thereby dysregulating the septal theta drive on the hippocampus and leading to cognitive impairment. In the context of AD, Martinez-Losa et al. (Martinez-Losa et al. 2018) showed that transplanting INs over-expressing Nav1.1 restores the behavior-dependent modulation of gamma oscillations and behavioral performance in hAPP transgenic mice.

To further understand the mechanisms linking Nav1.1 expression to cognitive deficits and examine the coordination hypothesis, we investigated the effects of SCN1A down-regulation on the CA1 microcircuit in vivo. Hippocampal activity is characterized by spatially modulated firing of hippocampal place cells and their temporal relationships with local theta (θ) and gamma (γ) oscillations. These oscillations enable multiple-timescale organization of place cell assemblies that reflect the temporal organization of spatial memory (Buzsáki 2002; Dragoi and Buzsáki 2006). CA1 place cells, integrators of inputs coming mainly from CA3 and entorhinal cortex (EC), are good indicators of temporal coordination within the hippocampus. Such synchronization is strongly regulated by GABAergic neurons (Klausberger and Somogyi 2008). We hypothesize that the Nav1.1 loss of function, by affecting INs, will impact synaptic integration and timing control of CA1 pyramidal cells, resulting in cognitive impairment independent of seizures. To test this hypothesis, we induced a down regulation of Nav1.1 in the dorsal hippocampus via an RNA interference-based approach. We show that focal, unilateral Nav1.1 knock-down (KD) in the dorsal hippocampus is sufficient to induce deficits in a spatial novelty task which are associated with a decrease in CA1 IN firing rate and phase locking to θ rhythm. These effects lead to alterations in temporal coding properties of pyramidal cells, such as phase precession and compression of ongoing sequences.

Materials and Methods

Overview

About 26 male Long–Evans black-hooded rats (300–350 g) were used for in vivo electrophysiology and behavior analysis. All behavioral, pharmacological, and surgical procedures were done in accordance with the National Institutes of Health guidelines and approved by the University of Vermont Institutional Care and Use Committee. About 14 rats were injected in the right dorsal CA1 with a lentivirus carrying a plasmid expressing GFP and the shRNA sequence (cf. Viral Vector Injections) targeting the *Scn1a* mRNA (Nav1.1 KD group). About 12 other rats were injected with a control lentivirus carrying only the plasmid expressing GFP (CTR group). Following 2 weeks of recovery, rats were tested in the elevated plus maze (EPM), open field, and a reaction to novelty task. After 1 week, rats were implanted with microdrives, and tetrodes were lowered in the CA1. The electrophysiological signal was recorded while rats were foraging for sucrose pellets in a circular open arena or running in a circular track. Recordings made in the circular open arena were used for basic place cell properties, stability, and phase locking. Recordings made in the circular track were used for phase precession analyses. Electrophysiological data from five CTR and three Nav1.1KD rats were not exploited because of poor recording quality. Animals were then sacrificed and perfused, and their brains were removed for histological analysis. Three Nav1.1 KD animals were excluded based on the qualitative histological criterion.

Viral Vector Injections

To induce a local KD of Nav1.1, we used a lentivirus carrying an FUGW plasmid expressing either GFP (CTR) or GFP and an shRNA sequence (5′—CCAGAGCGATTATGTGACAAGCATT—3′) targeting the *Scn1a* gene and driven by a U6 promotor as previously described (Bender et al. 2013, 2016). This sequence was chosen because it was the most efficient to reduce Nav1.1 expression in cultured cell lines and in vivo (Bender et al. 2013). Rats were anesthetized with isoflurane (1.5–3%) and lentiviral vectors were injected into the CA1 pyramidal cell layer of the right dorsal hippocampus. Rats were divided in two groups: a CTR group injected with control viral vector and an Nav1.1 KD group injected with the viral vector containing the shRNA sequence against *Scn1a*. A total of 4 µL of the viral solution were injected through four injection sites (1 µL per site) at the following coordinates respective to bregma (Paxinos and Watson 2007) (Antero-Posterior: −3/−3.5 mm, Median-Lateral: −2/−2.5 mm, Dorso-Ventral: −3/−2.5 mm) (Fig. 1A). Rats were then allowed 2 weeks of recovery.

Behavior

Behavior was recorded in a 3 m by 4 m room via a USB camera placed on the ceiling, above the apparatus. Tests were performed according to the following sequence.

Open field consisted of a gray painted circular arena (70-cm diameter × 50-cm height). Rats were placed in the center of the arena and left to explore freely for 15 min. Distance traveled and latency to the center zone (defined as a 20-cm diameter) were measured during the first 5 min.

EPM consisted of a 42 × 42 cm plus shaped maze with two of the four arms (East and West facing arms) closed by 40.5-cm high walls. For each trial, rats were placed in the center of the maze

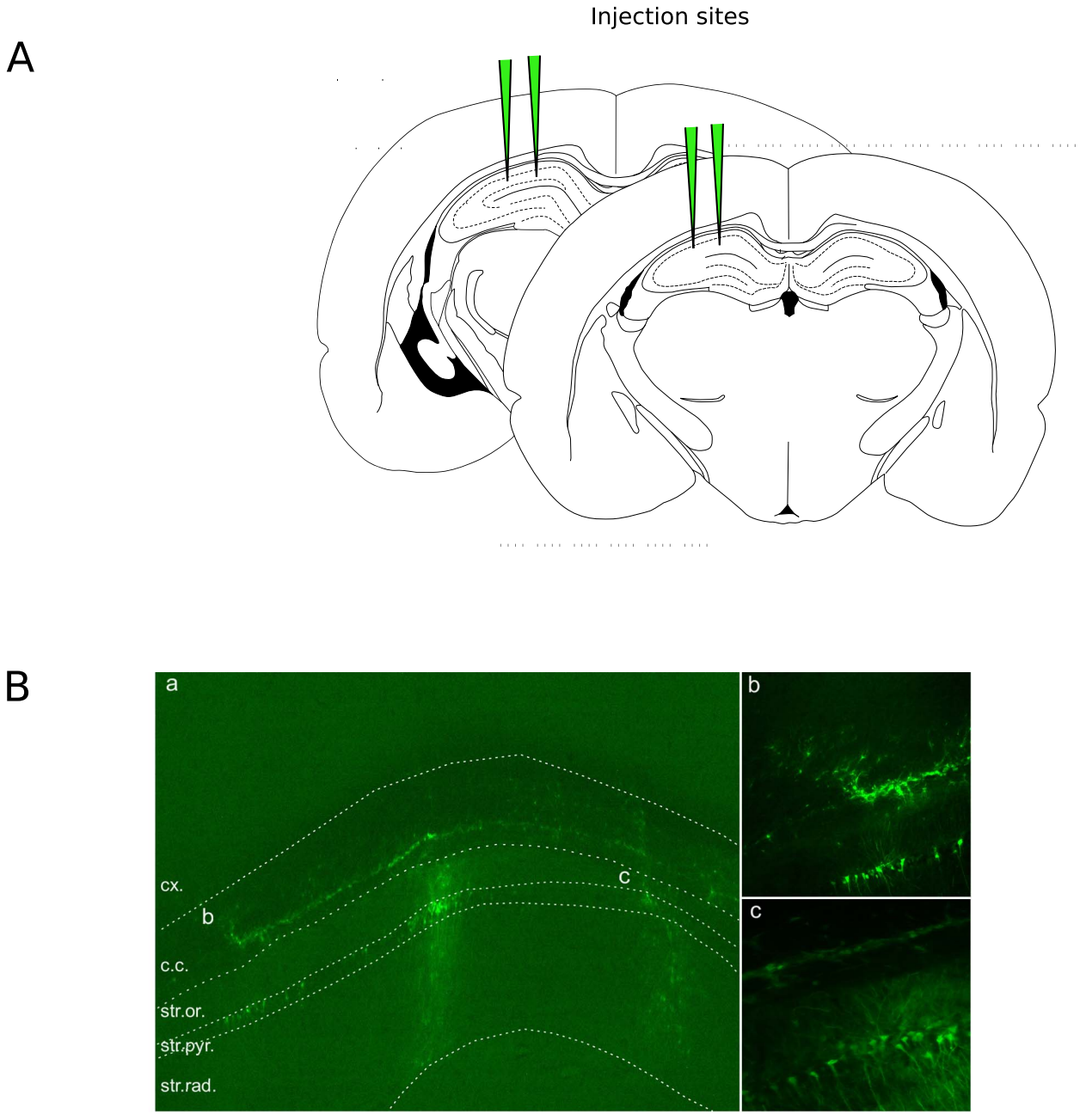

Figure 1. Viral vector injection and expression. (*A*) Schematic representation of the four injection sites targetting the rigth hippocampal CA1 region. (*B*) Example of CA1 expression in an Nav1.1 KD rat. (*a*) CA1. cx, cortex; cc, corpus callosum; str.or, stratum oriens; str.pyr, stratum pyramidale; str.rad, stratum radiatum. (*b* and *c*) Enlarged views of two regions from (*a*).

facing one of the closed arms. The time spent in closed and open arms was measured for the first 5 min of the trial.

Reaction to novelty task apparatus consisted of a 70×70 cm square-shaped arena with 50-cm high walls. Rats were first habituated to the apparatus for 15 min and exposed to a baseline configuration where two different objects were placed in zones A and C as shown in Figure 1B (Expo.). Rats were then returned to their home cage for 5 min, while one of the objects was moved to a new location (Zone B). Rats were placed back in the arena and allowed to explore this novel spatial configuration for 15 min (Test 1: reaction to spatial change). In the following session, the object in zone C was replaced by a new object and rats were allowed to explore again for 15 min (Test 2: reaction to object change). The time spent exploring each zone (defined as the time spent within a 10-cm radius from the object center) was measured during the first 5 min of each session. Performance was measured via a discrimination index (DI) expressed as the time spent near the object of interest divided by the sum of the time spent near the three possible zones. T_A, T_B, and T_C correspond to the time spent in zones A, B, and C, respectively. Referring to Figure 1B, we defined as $DI = T_B/(T_A + T_B + T_C)$ for Test 1 and $DI = T_C/(T_A + T_B + T_C)$ for Test 2.

Electrophysiological Recording

Two weeks after the first surgery, rats were implanted with eight drivable tetrode microdrives (Versa Drives, Neuralynx) in the hippocampus (CTR, $N = 8$; Nav1.1 KD, $N = 7$) under 3–5% isoflurane anesthesia (Lenck-Santini and Holmes 2008). A bigger craniotomy was performed at the same coordinates as for the viral vector injections and the electrodes aimed at the superficial layer of the neocortex (−1.5 mm below dura).

One week later, tetrodes were progressively lowered into the CA1 region of the dorsal hippocampus over a period of a week until the tetrodes reached the cell layer. Rats were trained to forage for food in a circular arena and run between the two ends of a circular track (ø: 90 cm, 300-cm long) for food reward (sugar pellet). Between each session, tetrodes were moved slightly (between 10 and 80 µm) to make sure that we recorded a different set of cells.

Data Acquisition

One red light emitting diode was mounted on the head stage to track the animal location. Position data were sampled at 30 Hz by a CCD camera. The signal from the electrodes was preamplified from the rat head by operational amplifiers mounted as followers. The signal was then transmitted through a cable and a rotating commutator. Both electrophysiological signal (0.1 Hz—32 KHz) and rat position were acquired on a Neuralynx acquisition system (Digitalynx SX and Cheetah software, Neuralynx).

Electrophysiological Data Analysis

Unit detection and extraction were performed off-line using a custom-built MATLAB® program (Mathworks). The signal from each of the four channels constituting a tetrode was filtered (300–9000 Hz), and unit activity (action potentials, APs) was extracted whenever the signal was larger than a threshold set above background activity (20–50 µV, i.e., 3 SD above the background noise level). To avoid detecting the same unit twice on the same tetrode, a 0.2-ms silent period was set until a new detection was possible. Unit discrimination was performed using Spike Sort 3D software (Neuralynx), and clusters that included cells firing within the 2-ms refractory period around each spike were discarded. To discriminate between putative pyramidal cells and INs (Fig. 2A), we used three parameters: mean firing rate (number of AP by second during 10-min recording session), AP width, and instantaneous firing frequency: that is, the inverse of the peak of the interspike interval (ISI) histogram. Typically, INs from the pyramidal cell layer and its vicinity fire at higher firing rates have narrower APs and larger mean ISI than pyramidal cells. To characterize bouts of higher activity in INs, we first binned spike trains in 5-ms bins, smoothed them using moving average filter with a 50-bin span. Peaks of higher activity were detected when firing exceeded 3 SD above the mean firing of the whole session. The duration of each peak was computed as the distance between the points to the left and right of the peak where the signal intercepts half the peak prominence (see findpeaks function in MATLAB®).

LFP power analysis was performed on 0.1–900 Hz filtered signals using multitaper Fourier transform (Chronux MATLAB® toolbox). For single-unit θ phase modulation, LFP signal was filtered after acquisition in the θ band (5–14 Hz) using a Chebyshev filter. Since θ phase and power vary as a function of depth across hippocampal CA1 (Buzsáki 2002), we had to ensure that tetrode and reference locations remained similar across different recordings and animals. For this reason, we selected only the recordings where tetrodes were in the stratum pyramidale (Str.pyr.) with a silent reference electrode located in the stratum oriens (Str. Or.). To obtain a precise measure for θ phase, we extracted theta episodes only when the θ/δ power ratio was >2.

Phase modulation of neuronal firing. θ phase locking: the θ phase of APs was interpolated from the Hilbert transform of the θ filtered LFP. For each neuron, phase distribution for all APs was constructed using 30° bin histograms (Figs 3 and 4); the strength of θ modulation was computed by constructing a vector from all AP phase distribution and computing its resultant length ($\overline{R}$). The preferred direction of AP firing was provided by its circular mean (Fisher 1993). Θ and γ modulation indices of individual cells were estimated based on the cells autocorrelogram as in Lopez-Pigozzi et al. (Lopez-Pigozzi et al. 2016). Only cells that fired more than 100 APs during the session were included. Autocorrelograms were substracted from the mean, and their power-spectral densities were estimated as the absolute value of their fast Fourier transform coefficients. θ and γ modulation indices were computed as the peak power between 6 and 11 Hz for θ and 40 and 90 Hz for γ divided by the quadratic mean of the total 1–40 Hz or 1–90 Hz spectrum.

Putative INs that showed significant θ modulation (as revealed by the Rayleigh test) were further separated into four classes (Fig. 3A) on the basis of their preferred firing θ phase during the pellet chasing task in the arena (Lopez-Pigozzi et al. 2016). Class 1 IN fired at the trough of θ (−15° to 15°), Class 2 at the rising phase (15–165°), Class 3 at the peak (165–195°), and Class 4 at the descending phase (195° to −15°).

Place cell spatial properties. In the circular arena, spatial coherence was used to estimate local smoothness of the spatial firing of pyramidal cells. A map (Fig. 5) was constructed using 3D histogram of firing rate relative to position (2 cm/pixel), divided by the time spent in each pixel. To assess the stability of place cells, two maps from consecutive sessions were compared pixel-by-pixel (Muller et al. 1987; Lenck-Santini et al. 2001). A correlation coefficient was calculated between the two maps and then the second map was rotated with increasing angles with the correlation coefficient recalculated for each angle. The correlation coefficient at 0° angle (R at 0°), the best correlation coefficient (R-max), and its corresponding angle were used as stability measures (Lenck-Santini and Holmes 2008).

θ phase precession. θ phase precession can be measured as a circular-linear correlation between the θ phase at which a place cell fires and the corresponding rat ongoing location (Fig. 6 A,B). In the circular track, laps were separated between clockwise and counterclockwise directions. The rat position in the track was linearized, and 2D firing rate histograms (2.8-cm pixels) were constructed (Lenck-Santini and Holmes 2008) (Fig. 5B) and smoothed using a nonparametric Kernel (2 bins) via a local weighted regression (Smoothing function, MATLAB®). Place field limits were defined as the first pixel where firing rate exceeded 20% of the firing peak (Schmidt et al. 2009).

Each AP was associated with a linearized distance in the circular track and with the ongoing θ phase. A circular-linear correlation coefficient between an individual neuron AP phase and distance was calculated for each single lap. Only laps where cells fired >5 APs and covered more than 50% of the place field area were considered for analysis (Fig. 6). For each cell,

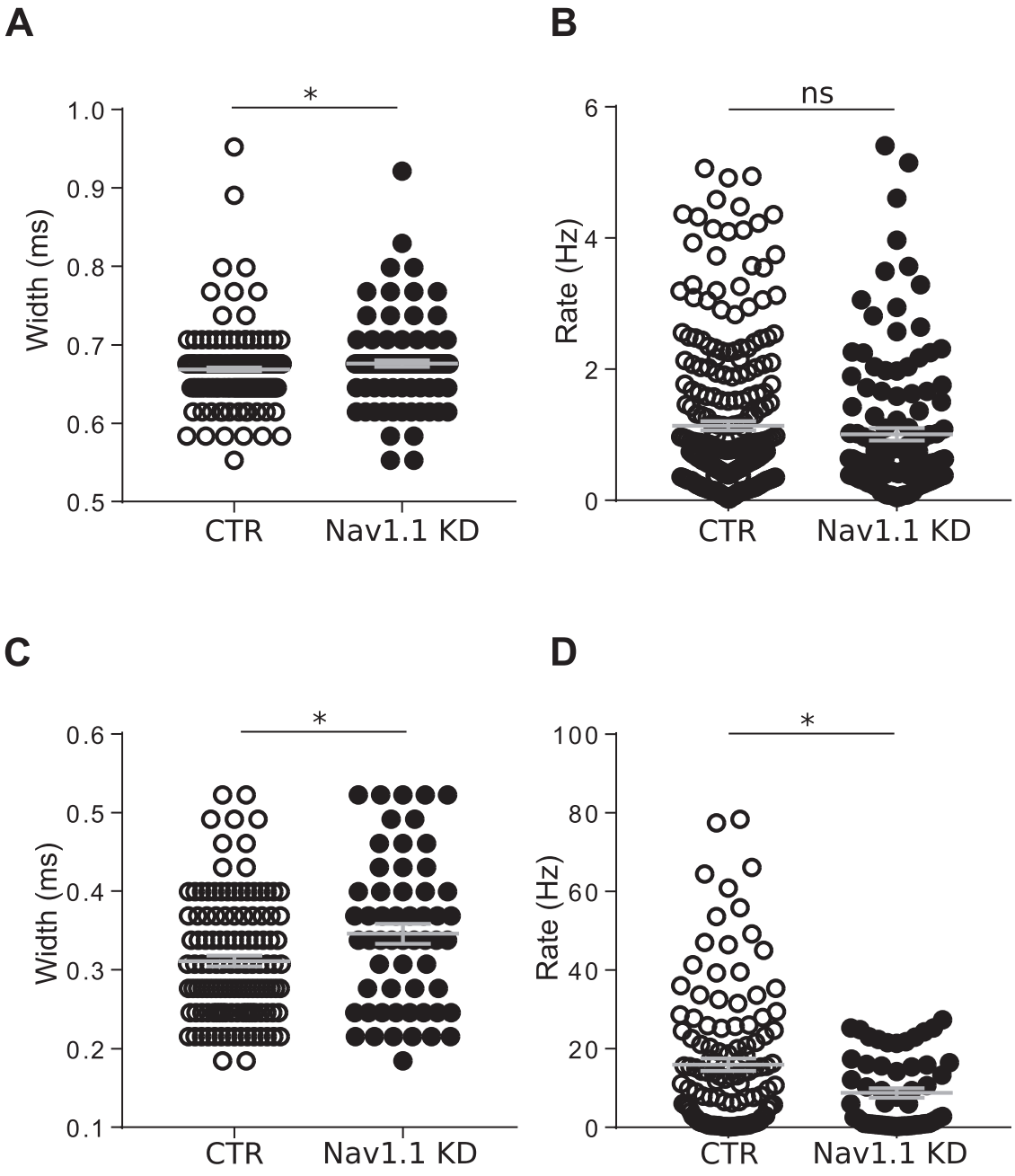

Figure 2. Nav1.1 KD changes the electrophysiological properties of INs. (*A*) Pyramidal cell width. (*B*) Pyramidal cell mean firing rate. (*C*) IN width. (*D*) IN mean firing rate.

we also estimated regression parameters between phase and distance. Because phase is circular by nature, we needed to avoid artificially breaking the continuity of the precession cloud. Here, phase values were shifted by 10° steps 36 times and regression was performed for each step. We selected the regression parameters that gave minimal dispersion values around the line (O'Keefe and Recce 1993). Among these parameters, the slope of the regression line provides an estimates of the rate at which precession occurs.

Θ sequence compression. Cross-correlograms (CCGs) (Dragoi and Buzsáki 2006) were constructed between the pairs of cells with overlapping fields in the circular track (Fig. 7A,B). CCGs were computed from binned spike times (3- and 1-ms bins for Real and Theta Time, respectively, see below) and normalized so that the autocorrelations at zero lag were identically equal to 1.0. Then, CCGs were filtered in two ways: 1) to detect the time it takes for the rat to go from one place field peak to another, CCGs were filtered with a 20-Hz low-pass filter. Under such filtering, the time at which the major CCG peak occurs corresponds to the time separating the peak activation of both cells (Real Time). 2) To detect the time separating APs of both cells within a θ cycle (Theta Time), CCGs were filtered using a 4–14 Hz bandpass filter. Here, Theta Time was estimated by the time difference between the local CCG peaks that are nearest to the zero lag. When Real Time values were positive, we used the positive peak time after the zero lag; when it was negative, we used the

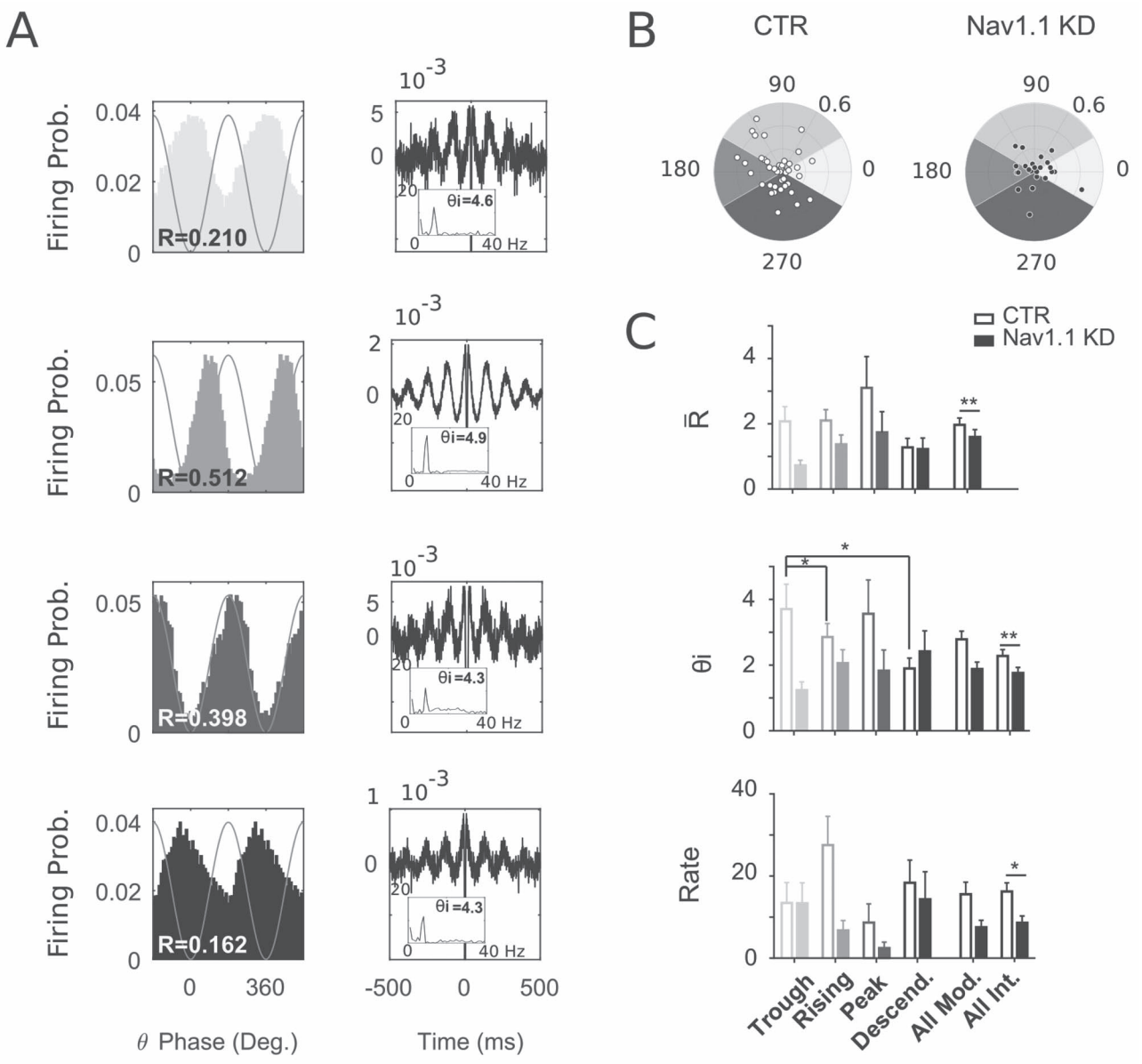

Figure 3. IN firing relationships with θ. (*A*) θ Phase histogram of four CTR INs preferentially firing at different θ phase and their autocorrelogram: INs were divided into four groups based on their θ phase preference. From top to bottom: trough, rising, peak, and Descending phase preference. (*A*) Distribution of preferred firing phase of the whole IN population in CTR versus Nav1.1 KD. (*B*) Mean value ($\overline{R}$), θi, and firing rate for each IN subpopulation. For $\overline{R}$ and θi, data are adjusted for the cell firing rate. Shades of gray correspond to the cell classes represented in (*A*) and (*B*). Descend: descending phase, All Mod.: INs with significant theta modulation, All Int.: all INs, including those that are not significantly theta modulated. GEE $^{*}P < 0.05$ $^{**}P < 0.01$.

negative peak time. For analysis, we selected only the pairs with CCGs showing a total probability of cofiring within a 1000-ms time window greater than 0.02. Theta ratio was computed as the Real Time/Theta Time. Theta modulation index was computed as the highest amplitude of the CCG histogram filtered at 4–14 Hz.

Statistical Analysis

Differences were considered significant when the *P*-value of each test was < 0.05.

Normality of distributions was tested using the Kolmogorov–Smirnov test.

For behavioral analyses, differences between groups were tested using *t* tests and discrimination indices for each group were compared to chance performance using one-sample *t* tests (Inostroza et al. 2013).

For in vivo single unit firing properties, place cell properties, and LFP data, differences between CTR and Nav1.1 KD group were evaluated using the Mann–Whitney test. The activity of a neuron was considered phase modulated when the *P*-value calculated with the Rayleigh test was ≤ 0.01. The Watson–Williams circular test was used to quantify differences of phase preference between CTR and Nav1.1 KD cell populations (Senior et al. 2008). We used generalized estimating equations (GEEs) (SPSS v24, IBM Corporation) to identify the impact of *Scn1a*

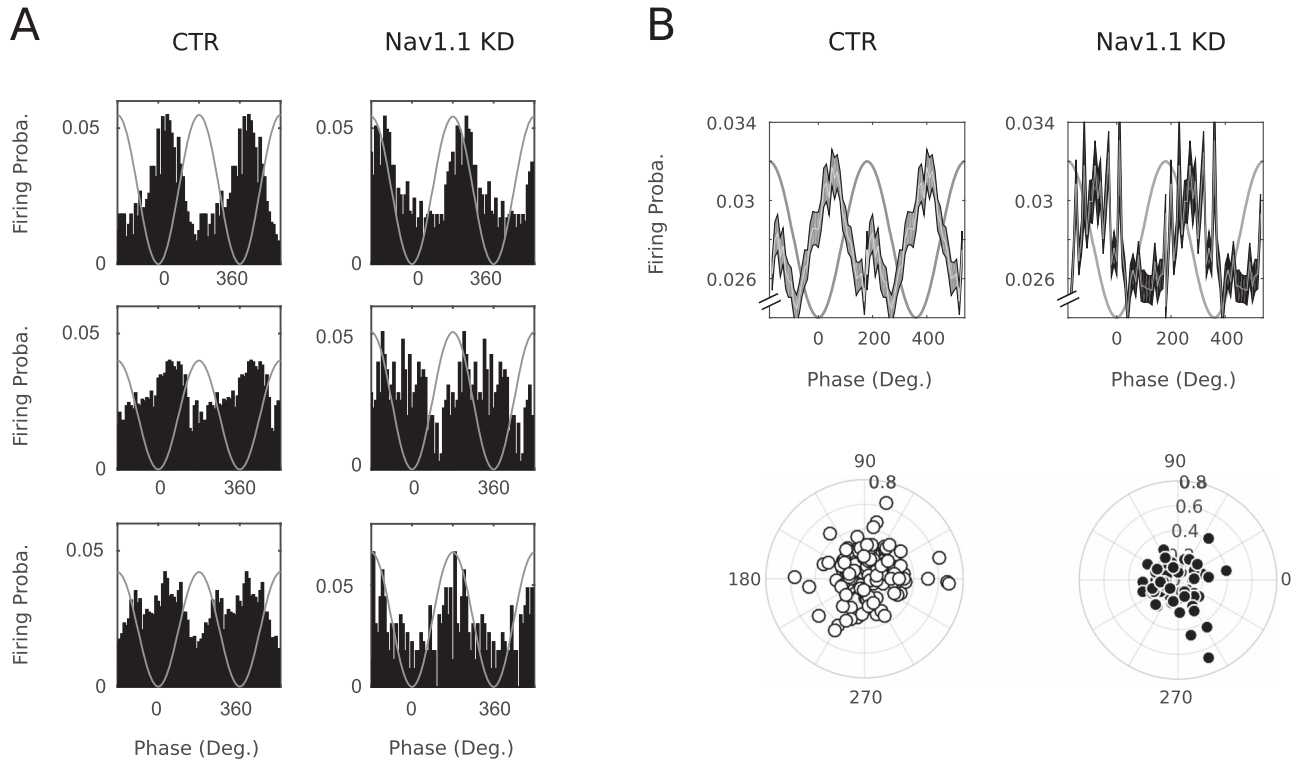

Figure 4. Pyramidal cell θ phase locking. (*A*) θ phase histogram of three different CTR and three different Nav1.1 KD pyramidal cells. (*A*) Normalized population phase histogram of the entire CTR and Nav1.1 KD pyramidal cell population. Distribution of the preferred firing phase of pyramidal cell population.

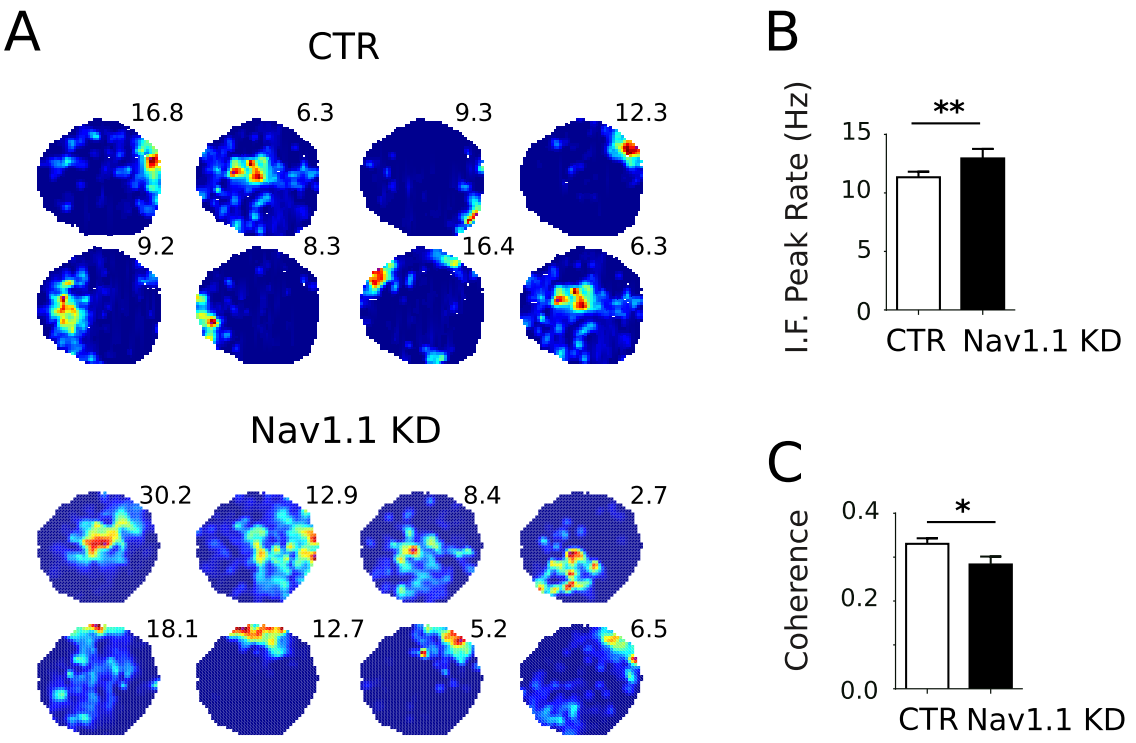

Figure 5. Nav1.1 KD affects CA1 place cell properties. (*A*) Rate map examples of eight simultaneously recorded Place cells in one CTR and one Nav1.1 KD animal. Individual peak firing rates (Hz) are shown above each map. (*B*) In-field (I.F.) peak firing rate, that is, the peak firing rate of individual place cells inside their place field is increased in the Nav1.1 KD group. (*C*) Coherence, that is, the correlation between the firing rate in each pixel and its neighbors, is decreased in the Nav1.1 KD group compared with the CTR group.

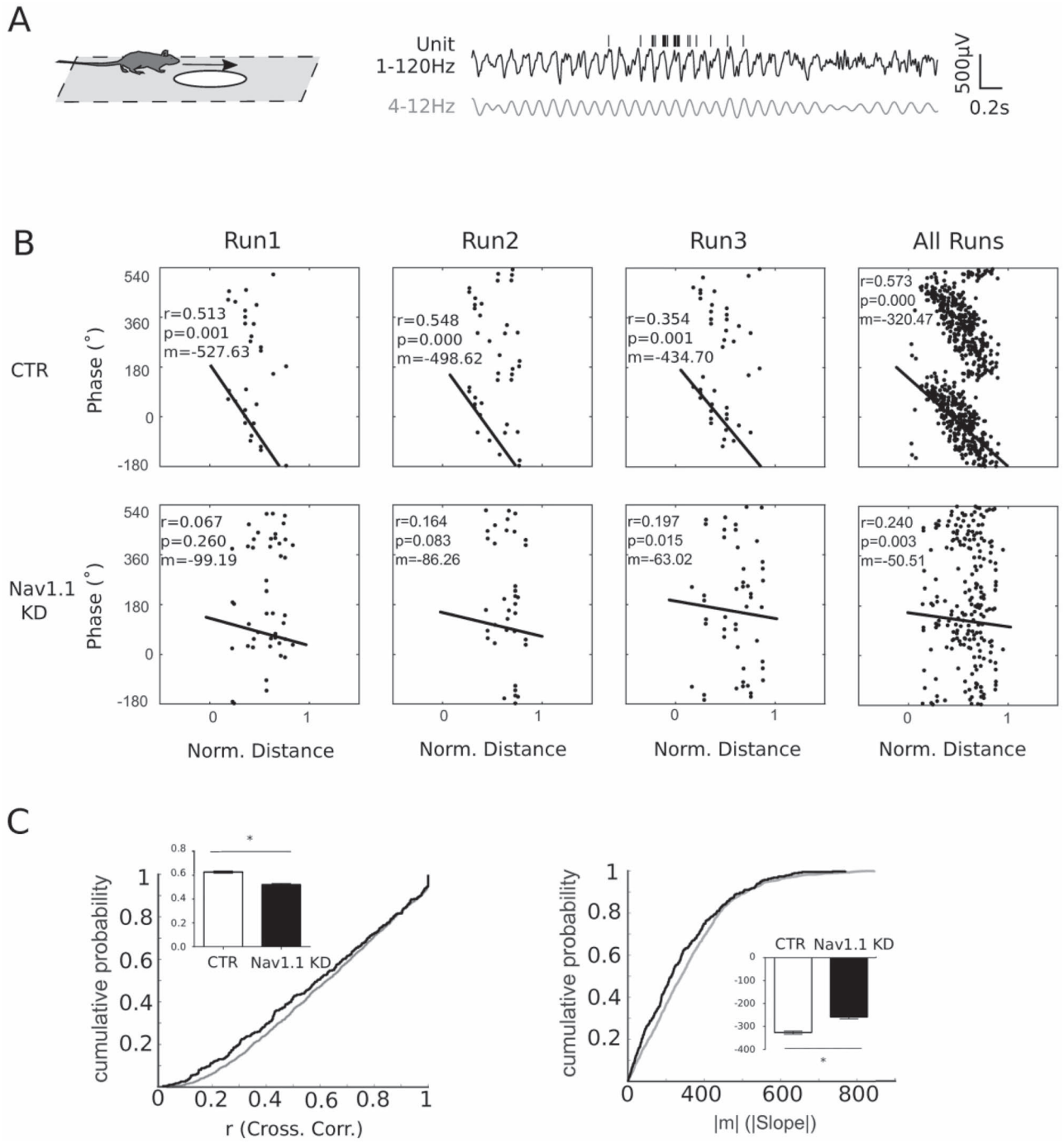

Figure 6. Nav1.1 KD alters place cell θ phase precession. (*A*) Illustration of place cell firing as the rat crosses its place field (left). The activity of a CTR place cell is represented on the right during a single run through the field (each vertical bar represents an AP) together with its relationship with the ongoing θ oscillation (bellow) filtered at different frequencies. (*B*) Phase-distance plots of the same cell in three individual runs in the same direction and for the whole session, all runs pooled (right). APs (black dots) are represented twice to improve display quality: once with their actual value, the second by adding 360° to their phase value. r: circular-linear correlation coefficient, m: slope of the phase-distance regression line (black line). (*C*) Cumulative distribution of r (right) and the slope (left) of both groups.

down-regulation on firing rate, θ and γ index across putative IN classes. We also fitted an interaction term to establish whether Nav1.1 KD had different effects, depending on the class of neuron.

For θ phase precession analysis and sigmoid relationship between Distance, Theta Time, and Real Time, we performed multivariable repeated measures regression analysis GEE in order to assume the correct distribution for the data and cluster for animals. The phase precession parameters were the dependent variable, and group (i.e., CTR or Nav1.1 KD) was the predictor. For Theta Time compression, Theta Time was the dependent variable and group was the predictor. Distance or Real Times were used as covariate.

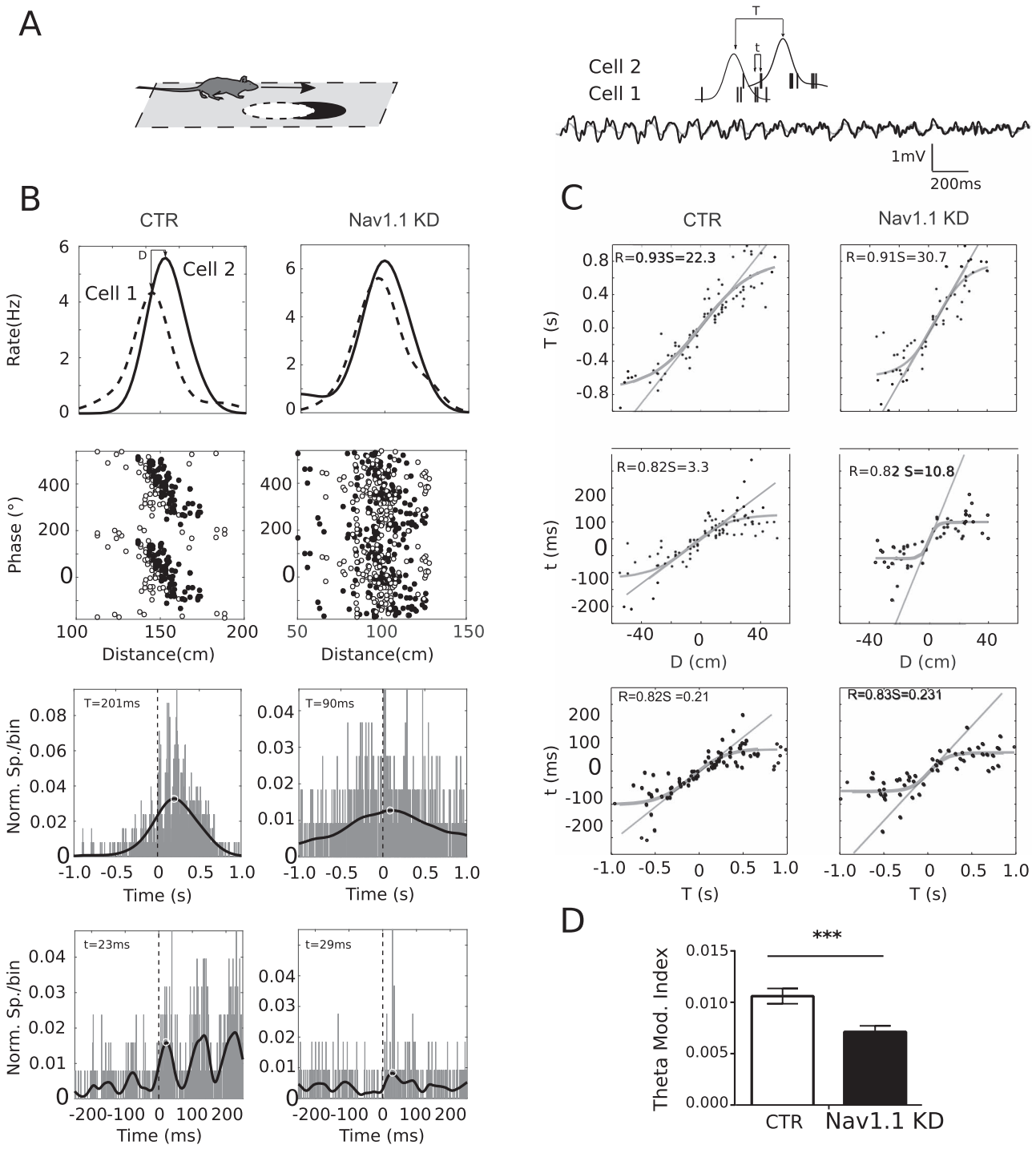

Figure 7. Nav1.1 KD impact place cell θ phase compression. (*A*) Firing activity of two simultaneously recorded place cells with overlapping fields and ongoing θ activity in the LFP. T: time it takes to run between the two peak fields, t: time separating APs in a single θ cycle. (*B*) Firing rate histograms (top), θ phase precession (middle), and CCGs (bottom two rows) of two pairs of place cells (CTR—left and Nav1.1 KD—right) with overlapping place fields. CCGs were performed on a Real Time scale (±1 s), with 3-ms bins, and filtered with a 2-Hz low-pass filter (second row from top) and also performed in the Theta Time (±250 ms) scale, that is, using a 14-Hz low pass filter and 1-ms bins. CCG peaks in Real Time and Theta Time scales are closest to zero correspond to T and t firing intervals, respectively, and these values were used in compression analysis. (*C*) Time compression of place cell sequences. Top row: relationship between inter-field distance (D) and real-time firing difference between cells (T). Middle row: relationship between D and theta-time firing interval between cells (t). Bottom row: real-time (T) versus theta-time (t) firing intervals. Note that, in CTR (left panel), these relationships follow a sigmoid curve that is wider and closer to a linear correlation than in Nav1.1 KD (right panel). (*D*) Mean CCGs θ modulation amplitude (Theta Mod. Index). CTR: $n = 87$ pairs, Nav1.1 KD: $n = 57$ pairs.

Histology and Immunofluorescence

To control for electrode placement, we performed immunofluorescence against GFP to detect the expression of the virus together with 4′,6-diamidino-2-phenylindole (DAPI) staining to visualize the scar left by the tetrodes. Rats were perfused with 0.09% NaCl solution followed by 4% paraformaldehyde (PFA)-NaCl solution. The brains were removed and postfixed in 4% PFA for 4–6 h and then put in a 30% sucrose solution. Brains were embedded in OCT, fast frozen using dry ice, and sections (20 µm) were cut with a cryostat. After 1 h incubation into blocking solution containing 0.1% triton, 5% natural goat serum, and 1% bovine serum albumin in a phosphate buffer saline (PBS) solution, slices were incubated overnight at 4°C with a rabbit anti-GFP antibody (Abcam, 1:1000 dilution). After three rinses with PBS, slices were incubated for 2 h at room temperature with a secondary Alexa 488 coupled goat anti-chicken antibody (ThermoFisher) and DAPI (1:1000 dilution each). The slices were then rinsed three more times with PBS before being mounted between slides and coverslips with Fluoromount mounting media (SigmaAldrich) (Fig. 1A).

Results

Viral Vector Expression Is Restricted to CA1

In order to KD the expression of Nav1.1 in hippocampal CA1 neurons, we performed stereotaxic injections of a virus expressing either an shRNA against *Scna1* and GFP or a control expressing GFP alone (Fig. 1A). We initially injected 12 CTR and 14 Nav1.1 KD rats. Immunohistochemical analysis revealed a heterogeneous spread of the virus among animals. Four Nav1.1KD animals were excluded based on qualitative histological criterion: either no GFP expression was observed in CA1 or GFP expression was detected in more than 10% of the DG neurons. We did not apply histological criterion to CTR, as the viral construction only expresses GFP and is not supposed to change neuronal activity. Expression in CA3 was never observed. In some cases, we observed minimal GFP expression in the DG and/or in the fibers of the corpus callosum (Fig. 1*Bb*, Supplementary Fig. 1). In addition, four CTR and three Nav1.1KD were excluded because of electrophysiological recording issues (head stage loss or absence of signal).

In vivo Nav1.1 KD INs Have Wider APs and a Lower Firing Rate

Single-unit recordings were performed 1 week after the implant surgery. Tetrodes were lowered progressively every day until the CA1 layer, characterized by sharp waves associated high-frequency oscillations (140–250 Hz), was reached. In 15 rats (eight CTR rats, seven Nav1.1 KD), 565 units have been recorded in the open circular arena. Based on their waveform and firing characteristics, 178 putative INs (122 CTR and 56 Nav1.1 KD) and 387 putative pyramidal cells (261 CTR and 126 Nav1.1 KD) have been identified. Given that IN waveforms were always recorded with the same tetrode as other pyramidal cells, their cell bodies were likely in the pyramidal cell layer or its direct proximity. This observation restricts the population to Cholesystokinin—CCK and PV expressing basket cells, axo-axonic, bistratified, and ivy IN subtypes.

Because Nav1.1 channels are involved in AP initiation and propagation, we hypothesized that Nav1.1 would affect AP waveforms. The AP width of putative INs was significantly larger in the Nav1.1 KD population than in CTR (Fig. 2C, Supplementary Table 1). To a lesser extent, pyramidal cell AP width was also increased (Fig. 2A).

In agreement with previous studies suggesting a role of Nav1.1 channels in sustaining fast-spiking activity, we found that the mean firing rate of INs was significantly decreased. For INs, there was a significant relationship between firing rate and AP width (GEE; Beta = −3.4, $P < 0.001$) and the nature of the relationship differed as a function of KD ($P = 0.012$) with a steeper decline in the Nav1.1 animals. Indeed, for Nav1.1 KD but not CTR INs, AP width was negatively correlated with firing rate (Nav1.1 KD: $r = -0.472$, $P < 0.001$; CTR: $r = 0.077$ ns). In any given cell, the increase of AP width and the efficacy of Nav1.1 KD are likely linked together. The observation that there is a correlation between AP width and firing rate is an indication that the decrease in firing rate is a direct consequence of Nav1.1 KD. We found no difference in signal quality between groups (Supplementary Fig.5).

Our data show that the mean firing rates and AP width remain very different between IN and pyramidal cells in mutants, despite Nav1.1 KD, suggesting that our classification criteria are still valid. The proportion of putative INs and pyramidal cells recorded is also similar between groups, again suggesting that we have not misclassified units.

However, IN instantaneous firing rate remained unchanged (Supplementary Table 1, Fig. 2D). To further investigate this change in IN firing, we detected for each cell bouts of increased firing activity (>3SD above the mean. See Materials and Methods). We found that the duration of such periods of increased firing was significantly lower in the Nav1.1 KD group (peak width: CTR: 293.9 ± 11.43 ms; Nav1.1KD: 254.7 ± 10.69 ms. *t*-test with Welch's correction: $t = 2.507$; $P = 0.013$, Supplementary Fig. 2). They did not differ in terms of number or normalized peak firing rate. Therefore, Nav1.1 KD INs failed to sustain prolonged firing as compared with CTR. In contrast, we did not find any difference in the mean firing rate nor the instantaneous frequency of pyramidal cells (Supplementary Table 1, Fig. 2A).

Our results therefore suggest that Nav1.1 KD specifically affects IN discharge while preserving pyramidal cell firing rate.

LFP Alterations of θ/γ Modulation in Nav1.1 KD Rats

LFP oscillations at θ and γ frequency and their interaction (i.e., cross-frequency coupling) in the hippocampus have been associated with cognitive performance and information processing (Lisman and Redish 2009; Amemiya and Redish 2018). While CA1 slow and fast γ rhythms reflect the influence of external origins (CA3 and EC, respectively) (Bieri et al. 2014), they are also intrinsically associated with both perisomatic and dendritic GABAergic activity (Mann et al. 2005; Buzsáki and Wang 2012; Lasztóczi and Klausberger 2014; Craig and McBain 2015). Since Nav1.1 KD changes IN activity, it is likely that γ oscillations or θ/γ coordination would also be altered. Interestingly, we did not observe any epileptiform activity nor interictal spikes throughout all electrophysiological recording periods.

There was no significant difference in θ power, peak frequency nor θ/γ ratio between groups (see Table 1 for statistics). In rodents, θ power and frequency are modulated by running speed (Richard et al. 2013). However, there was no difference in speed-θ frequency or speed-θ power correlations (Table 1).

We found no significant difference in γ amplitude or θ–γ power–power co-modulation indices (Supplementary Fig. 3*A*,*B*).

Table 1 LFP properties in the circular track (values are expressed by mean ± SEM, *P*-value: GEE)

	N	*n* sessions	θ/γ ratio	speed (cm/s)	θ frequency/speed (cm^{-1})
CTR	5	19	3.8 ± 0.4	29.3 ± 1.9	0.13 ± 0.02
Nav1.1 KD	5	14	3.2 ± 0.4	26 ± 3.2	0.19 ± 0.04
P-value			0.246	0.393	0.188

Position in the text: results section-LFP alteration of theta/gamma modulation in Nav1.1 KD rats section-end of second paragraph (p.18).

However, θ phase-γ amplitude coupling was weaker in Nav1.1 KD than in CTR rats for both slow and fast γ (slow γ modulation index, CTR: 0.23 ± 0.03, Nav1.1 KD: 0.11 ± 0.03, $P = 0.015$, fast γ modulation index, CTR: 0.14 ± 0.02, Nav1.1 KD: 0.0 8 ± 0.02, $P = 0.034$ GEE; Supplementary Fig. 3C).

In summary, Nav1.1 KD induced specific alterations of θ/γ co-modulation but no change in θ rhythm. These results confirm the contribution of IN activity to θ-γ cross-frequency coupling.

Decreased θ Modulation of IN Firing in Nav1.1 KD Rats

For unit analyses that are related to oscillations, we restricted our cell population exclusively to cells recorded with a silent reference electrode located in the Str. Or. (See Materials and Methods).

Different CA1 pyramidal cell and IN subtypes have been shown to fire at a specific phase of θ oscillations (Klausberger and Somogyi 2008; Mizuseki et al. 2009). Here, we classified INs based on their preferred θ firing phase into four groups (Fig. 3A,B): those that preferred firing in the trough of θ (CTR: $n = 8$; Nav1.1: $n = 8$), the upstroke (Rising. CTR: $n = 17$; Nav1.1 KD: $n = 9$), at the peak (CTR: $n = 4$, Nav1.1 KD: $n = 3$), and on the down stroke (Descending: CTR: $n = 12$; Nav1.1 KD: $n = 5$). Overall the proportion of cells in each class is not significantly different between groups ($\chi^2 = 1.7$; $P = 0.63$).

Using GEE including the effect of Nav1.1 KD with neuronal class and firing rate as covariates, we found that Nav1.1 KD IN firing rate was reduced in comparison to CTR INs (CTR: 15.6 ± 2.9 Hz; Nav1.1 KD: 7.5 ± 1.7 Hz; $P = 0.014$). There was no significant interaction between group and IN class ($P = 0.13$). We also found that the amplitude of θ modulation of the cell firing rate (θ index, θi) was reduced in Nav1.1 KD INs (GEE; 0.2 ± 0.02 in CTR; 0.12 ± 0.016 in Nav1.1 KD: $P = 0.004$). There was no significant interaction between group and IN class ($P = 0.15$). Because the computation of the θi depends on the number of APs emitted by the cell, it is influenced by the cell firing rate. This was also confirmed by our GEE approach where rate significantly influenced θi ($P < 0.001$). We therefore included a correction for firing rate as a confounder in our θi analyses. After adjusting for firing rate, θi was still reduced in Nav1.1 KD INs (CTR = 2.89 ± 0.3; Nav1.1 KD = 1.88 ± 0.23 in; $P = 0.008$). There was a significant interaction between group and IN class ($P = 0.014$), with the effect of Nav1.1 KD on θi being different between Trough firing-IN versus Descending-IN or Rising-IN (Fig. 3C).

In contrast, there was no effect of Nav1.1 KD on IN modulation by γ oscillations (data not shown) and ripple modulation of unit firing did not differ between groups (Supplementary Fig. 4).

To summarize, θ modulation of single unit firing was decreased in Nav1.1 KD INs. This alteration was different depending on the subclass of IN considered.

Nav1.1 KD Changes Pyramidal Cell Preferred θ Firing Phase

While CTR pyramidal cells were more likely to fire during the rising phase of local θ oscillation, Nav1.1 KD pyramidal cells preferentially fired during the descending phase (Fig. 4A,B; CTR: 60.2° ± 13° = 0.18 ± 0.008; Nav1.1 KD 251.5° ± 38° = 0.17 ± 0.012, $P < 0.001$ William–Watson test). As previously shown (Mizuseki et al. 2009), we observed a variability in terms of preferred θ firing phase within CA1 cells (Fig. 4B, left, top, and bottom).

Alteration of Nav1.1 KD Place Cell Properties

IN activity is critical for the regulation of place cell activity (Grienberger et al. 2017). Since Nav1.1 KD affects IN firing properties, we investigated the consequences of such alterations on place cell properties (Fig. 5, see Table 2 for statistics). Pyramidal cell spatial coherence was significantly decreased in the Nav1.1 KD population. Although place field size was not affected, the peak firing rate within the field was significantly increased (Table 2). Place cell stability, measured as the correlation coefficient between rate maps constructed from two consecutive sessions (see details in Materials and Methods) was not different between the two groups (Table 2).

Reduced θ Phase Precession of Nav1.1 KD Place Cell Firing

To assess whether changes in IN firing properties could affect pyramidal cell temporal organization, we investigated θ phase precession (O'Keefe and Recce 1993; Skaggs et al. 1996; Dragoi and Buzsáki 2006). Single unit recordings were performed in rats

Table 2 Place cell properties in the circular open arena (values are expressed as mean ± SEM, *P*-values were obtained using the Mann–Whitney test)

	N	*n*	Coherence	Place field size (cm2)	In field peak firing rate (Hz)	R-max*	R at 0°**
CTR	7	169	0.331 ± 0.013	148 ± 12.34	4.34 ± 0.15	0.273 ± 0.012	0.17 ± 0.01
Nav1.1 KD	7	59	0.283 ± 0.018	133.4 ± 14.13	5.18 ± 0.35	0.282 ± 0.016	0.2 1 ± 0.02
P-value			0.021	0.391	0.047	0.347	0.07

Position in the text: results section-alteration of Nav1.1KD place cell properties section-end of first paragraph (p. 20).
*R-max: correlation coefficient maximum between two maps.
**R at 0°: correlation coefficient without rotation.

Table 3 Place cell properties in the circular track (values are expressed by mean ± SEM, *P*-value: Mann–Whitney test)

	N	*n*	Place field size (cm)	# place field/cell
CTR	5	144	31.4 ± 0.4	1.19 ± 0.4
Nav1.1 KD	5	66	31.7 ± 2	1.26 ± 0.4
P-value			0.96	0.34

Position in the text: results section-reduced phase precession of Nav1.1 KD place cell firing section-end of first paragraph (p. 20).

running in a circular track (Fig. 6A,B). Here, five CTR and five Nav1.1 KD rats were used and 376 units were recorded (250 CTR and 126 Nav1.1 KD). About 210 place cells were recorded in the track (144 CTR and 66 Nav1.1 KD, see Table 3). As for the open circular arena, there was no difference in place field size or in the number of place fields per cell (See Table 3, CTR 17% having 2 fields, Nav1.1 KD 26% having 2 fields, Fisher exact test, ns). For further analysis, we only selected place fields with >50 AP per direction (CTR: 186 fields in 85 cells, Nav1.1 KD: 51 place fields in 46 cells).

On a session-by-session basis, θ phase precession was altered in the Nav1.1 KD group as compared with CTR. The mean correlation coefficient by group was decreased (CTR: 0.448 ± 0.022, Nav1.1 KD: 0.390 ± 0.025, $P = 0.016$, GEE on Fischer transform), and the slope of the linear-circular regression line was also decreased (CTR: −122.9 ± 6.3, Nav1.1 KD: −105.2 ± 4.6, $P = 0.036$, GEE). It has been shown that measuring θ phase precession on a trial-by-trial basis gives a better measure of the phase precession quality and reliability (Mehta et al. 2002; Schmidt et al. 2009; Feng et al. 2015) (Fig. 6B). The percentage of trials with a significant θ phase precession was significantly decreased in the Nav1.1 KD group (CTR: 464/1071 trials, 43.3%, Nav1.1 KD: 260/725 trials, 35.8%. Chi-square = 10.11 $P < 0.01$). The mean correlation coefficient by group was decreased (CTR: 0.625 ± 0.008, Nav1.1 KD: 0.522 ± 0.010, $P < 0.05$, GEE on Fischer transform). The slope of the linear-circular regression line was also affected (CTR: −326.58 ± 6.76, Nav1.1 KD: −258.77 ± 7.92, $P < 0.05$, GEE performed on the square root of the slopes to ensure normality, see mean and cumulative distribution on Fig. 6C).

Θ phase precession was observed in IN both in CTR and Nav1.1 KD groups. However, the quantitative comparison of IN phase precession between groups could not be performed because of the following biases. On the one hand, IN have multiple place fields that can only be detected based on phase precession patterns (Maurer et al. 2006). On the other hand, phase precession is normally quantified within place field limits, which cannot be uniquely delineated from firing rate changes in INs. That said, visual inspection of phase precession patterns for INs suggested that they did not differ between groups.

In summary, θ phase precession was altered in Nav1.1 KD pyramidal cells but could not be assessed in INs.

Loss of θ Sequence Compression between Nav1.1 KD Place Cells

To further study the temporal coding alterations, we looked at θ sequence compression by performing CCGs between pairs of place cells with overlapping fields (see Materials and Methods, Fig. 7A,B). We observed no difference in the mean compression factor between groups (CTR 10.8 ± 1.3, Nav1.1 KD 11.1 ± 1.7 $P = 0.877$, ns). However, the shape of the sigmoid that fits Real Time lag with Theta Time lag or the distance with Theta Time lag differed significantly (Interaction Group∗Real Time lag: $P < 0.0001$, Group effect: $P = 0.011$; Interaction Group∗Distance: $P = 0.013$, Group effect: $P = 0.037$, GEE; Fig. 7C). Similarly, the slopes of the associated linear correlation in the central region differed between groups (CTR slope = 0.1207 ± 0.02, Nav1.1KD slope = 0.09393 ± 0.02). In the Nav1.1 KD group, the linear part of the sigmoid only spans small distances, suggesting a failure to encode longer distances within a θ cycle. Finally, the θ modulation of CCGs was weaker in Nav1.1 KD than in CTR pairs (CTR index = 0.0106 ± 0.0007, Nav1.1KD index = 0.007 ± 0.0006, $P < 0.0001$, Fig. 7D).

Decreased Performance in the Reaction to Spatial Novelty Task

We investigated the effect of the focal, dorsal CA1 Nav1.1 KD on behavioral performance. Behavioral assays were performed 2 weeks after viral vector injections. Results are presented in Figure 8.

Open field (Fig. 8A) and EPM (Fig. 8B) were done to assess locomotor activity and anxiety level. In both tests, distance traveled did not differ significantly between CTR and Nav1.1 KD rats. In the open field, the latency to- and time spent in the center zone did not differ between groups. There was no difference in the number of entries in open versus closed arms in the EPM. Finally, during the first exposure to the reaction to novelty task apparatus (Expo), distance traveled did not differ between groups. Therefore, Nav1.1 KD rats did not exhibit locomotion deficit or stress and anxiety behavior (Fig. 8D).

In the second session of the reaction to novelty test (Test 1: Spatial change, "Where"), CTR rats showed a preference for the moved object, with a tendency to spend more time exploring in zone B compared with zone C [one-way ANOVA, $P < 0.001$, Tukey's multiple comparison, (B vs. A) $P < 0.001$, (B vs. C) $P = 0.122$, (A vs. C) $P < 0.05$]. In contrast, Nav1.1 KD rats showed no preference for any location. The place DI was significantly higher in CTR than in Nav1.1 KD rats (Mann–Whitney test, $P = 0.0159$); the Nav1.1 KD rats performed at chance level ($t = 1.09$, $P = 0.33$, ns), while CTR group was significantly better than chance ($t = 6.5$ $P < 0.005$, Fig. 8D). In the third session (Test 2: reaction to identity change; "What"), both groups increased their exploration of zone C. Place DI and the object recognition index showed no differences between CTR and Nav1.1 KD groups (CTR: $t = 5.8$, $P < 0.005$, Nav1.1KD: $t = 4.5$, $P < 0.05$, Fig. 8E).

Altogether, these results suggest that Nav1.1 KD rats had a specific spatial memory deficit but that memory for objects, which is not hippocampal dependent, was intact.

Discussion

In this study, we show that focal, unilateral Nav1.1 down-regulation in a portion of dorsal hippocampus impairs the

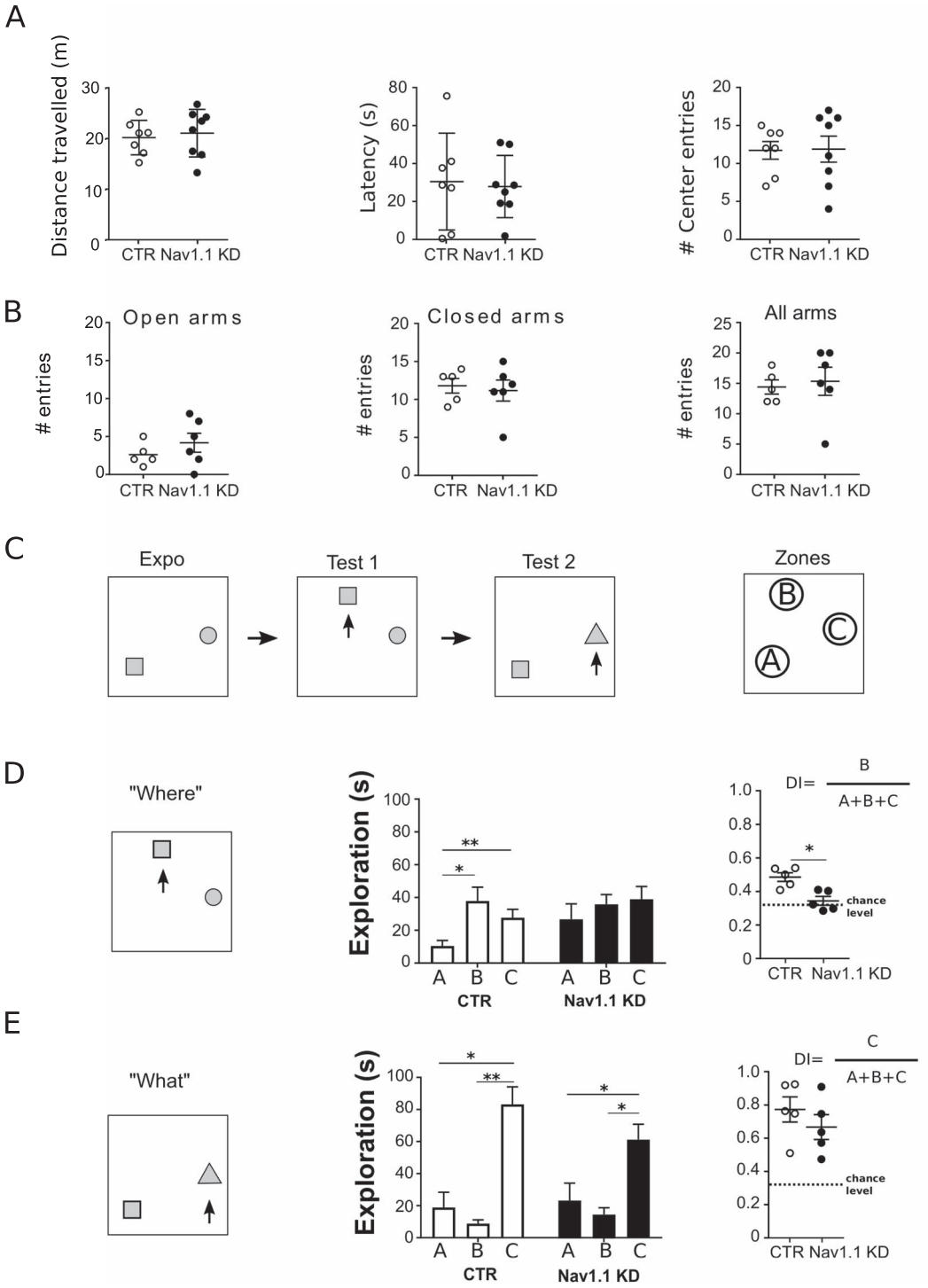

Figure 8. Nav1.1 KD impairs performance on a reaction to novelty task. (*A*) Open field. Left panel: number of entries in the center zone. Middle panel: Latency to reach the center zone. Right panel: number of entries in the center zone. (*B*) EPZ. Left panel: number of entries in open arms. Middle panel: number of entries in closed arms. Right panel: total number of entries. (*C*) Reaction to novelty experimental procedure. Expo: exposure to the environment. Test 1: reaction to spatial change, one object is moved. Test 2: reaction to object change, one object is replaced by a new object. A–C zones represent the area where the exploration time is quantified. (*D*) Reaction to spatial change ("Where"). Middle panel: mean time spent in each zone during Test 1. CTR ($N = 5$), Nav1.1 KD ($N = 5$). Right panel: DI. DI is significantly reduced in Nav1.1 KD group compared with CTR. (*E*) Reaction to object change ("What"). Middle panel: mean time spent in each zone during Test 2. Rigth panel: DI is not different between both groups. (*F*) $^{*}P < 0.05$, *t*-test.

reaction to spatial novelty, place cell quality, phase precession, and temporal compression, processes believed to be critical for the organization of spatial memory representations.

Overall, our results confirm the hypothesis that Nav1.1 plays a vital role in cognitive impairment, independently of other confounding factors associated with neurological disorders such as AD or DS. These findings lend support to the idea that treatments targeting Nav1.1 expression or function in these syndromes could be a valuable therapeutic target (Jensen et al. 2014; Martinez-Losa et al. 2018).

Nav1.1 KD Affects IN Activity

In the central nervous system, Nav1.1 is expressed in both GABAergic neurons and pyramidal cells; however, alterations in its expression are believed to affect mostly the excitability of INs (Yu et al. 2006; Ogiwara et al. 2007; Cheah et al. 2012; Dutton et al. 2013) by decreasing their capacity to produce APs at high frequency or under strong depolarization.

It has been shown that both PV and somatostatin (SOM) INs express Nav1.1 and that their firing properties are affected by Nav1.1 alteration (Tai et al. 2014). In agreement with the literature, we found that Nav1.1 KD induced by RNAi in vivo affects the intrinsic firing properties of INs. Following Nav1.1 KD, putative INs isolated based on their waveform morphology showed a decreased firing rate and a weaker θ phase modulation. In turn, pyramidal cells fired at an opposite θ phase than expected had a weaker θ phase precession and an abnormal compression of temporal sequences. We propose that such changes in pyramidal cell firing dynamics are the consequence of IN dysfunction.

It is still unclear whether and how Nav1.1 KD directly affects pyramidal cells in pathological conditions. In rodent models, while Nav1.1 is expressed in pyramidal cells, its loss of function appears to have no electrophysiological consequence on freshly dissociated pyramidal neurons from heterozygous Nav1.1 KO mice (Yu et al. 2006). This is not surprising since physiologically, pyramidal cells do not fire at high frequency and only fast spiking activity seems to be affected by Nav1.1 KD. On the other hand, the seizure phenotype is more severe in mice carrying a targeted Scn1a deletion in GABAergic IN than in constitutive knockout mice. This suggests that, when pyramidal cells are driven to fire at high frequency under pathological conditions, Nav1.1 deficits in pyramidal cells may have a seizure protective effect (Cheah et al. 2012). Yet studies using human induced pluripotent stem cells derived from DS patients have shown mixed results. Some studies show that excitatory cells have increased sodium current (Liu et al. 2013), whereas others, more in accordance with rodent models, suggest a disinhibition mechanism (Han et al. 2012; Higurashi et al. 2013). Our results, showing a selective decrease in IN but not in pyramidal cell firing rate, also support the idea of disinhibition following Nav1.1 down-regulation.

Hippocampal INs form a highly heterogeneous family with distinct physiological and network properties. Owing to these properties, each subclass plays a specific functional role in the network. For instance, fast-spiking, perisomatic-projecting INs directly influence the timing of pyramidal cell discharge, while dendritic-targeting INs influence inputs to the cell. Interestingly, IN subclasses are differentially modulated by θ oscillations. While some INs are not modulated by θ oscillations (Czurkó et al. 2011), others such as PV-, CCK-basket cells, Oriens-Lacunosum Moleculare (OLM), or bistratified cells fire at specific phases of θ. It is therefore believed that each subclass differentially influences hippocampal network dynamics thereby affecting information processing. By extension, there is growing evidence that alterations of specific IN types could have important network and behavioral consequences. For example, in animal models of temporal lobe epilepsy (Lopez-Pigozzi et al. 2016), it has been shown that hippocampal PV IN properties are altered and that such alteration are associated with θ and γ rhythm disturbances as well as episodic memory deficits. Computational models and in vitro studies suggest that both IN activity and the local θ phase at which they discharge are critical. Indeed, these parameters determine the temporal organization of inhibition into the different pyramidal cell compartments, thereby modulating pyramidal cell activation and synaptic plasticity via spike timing dependent plasticity (Cutsuridis and Hasselmo 2012; Lovett-Barron et al. 2012; Hasselmo and Stern 2014). In favor of this hypothesis, in vivo optogenetic silencing of PV INs (Royer et al. 2012) induces changes in place cell firing rate inside but not outside the place field and shifted the preferred θ phase of the place cell from the peak to the trough. In contrast, SOM IN silencing specifically altered pyramidal cell bursting properties. Since histological and morphological IN subtype identification is not possible in extracellular recordings, we can only speculate about the IN subtype being recorded. Likewise, we do not have control over the neuronal types being infected by the RNAi viral vector and it is possible that INs in the Str. Radiatum or Str. Lacunosum Moleculare have also been infected and may affect circuit coordination. Nevertheless, the INs we recorded concomitantly with pyramidal cells in CA1 were likely located in the Str. Pyramidale and to a certain extent in the Str. Oriens, restricting their possible identity to specific basket cells, axo-axonic, bistratified, and ivy cells. The putative INs that we recorded were individually found to fire preferentially at various phases of θ, reflecting their heterogeneity. While the proportions of cells found in each phase category did not change significantly, there was a noticeable reduction in the number of cells recorded in Nav1.1 KD animals, particularly in the IN subtypes firing at the rising and descending phases of θ (likely CCK and PV basket cells, respectively). There was also an overall decrease in firing rate and θ modulation in remaining INs. In addition, Nav1.1 KD induced an increase in the firing rate of pyramidal cells selectively inside but not outside place fields and a shift of pyramidal preferred phase towards earlier phase, a result similar to those of Royer et al. (Royer et al. 2012) after PV IN optogenetic inactivation. We did not observe any change in pyramidal cell bursting, suggesting an intact SOM IN activity. However, interpreting changes in the firing properties of specific cell types in functioning/in-vivo networks are also difficult because each neuron subtype interacts with other subtypes both directly and indirectly (Acsády et al. 1996; Tsodyks et al. 1997; Stark et al. 2013). In addition, it is possible that, such as pyramidal cells, IN subtypes changed their preferred firing phase after Nav.1.1 KD, therefore falling in a different category.

The modulators of θ frequency and amplitude are located outside CA1 (Vertes et al. 2004). We only targeted CA1 for Nav1.1 KD; it is therefore likely that the differences observed in single unit θ phase modulation are not caused by extrahippocampal deficits nor by a bias in θ phase extraction in one group compared with the other but rather by intrahippocampal Nav.1.1 reduction.

Nav1.1 KD Affects Pyramidal Cell θ Phase Precession and Phase Compression

Place cell θ phase precession was observed in fewer place cells and in fewer trials after Nav1.1 KD. The slope and the correlation coefficient of the circular-linear regression also decreased. CA1 θ phase precession is a complex phenomenon, likely depending on two major components (Fernández-Ruiz et al. 2017). The first component is the dual but delayed influence of CA3 and EC inputs to the pyramidal cell. The second component is the delayed effect of OLM and PV IN modulation on distal dendrites versus proximal dendrites and soma of pyramidal cells, respectively. Under this view, INs mainly modulate EC and CA3 inputs and, therefore, the shape of the precession. In our case, since we induced a focal Nav1.1 KD in CA1 and that both EC and CA3 were not infected, we can rule out a direct Nav1.1 KD effect on the first component. However, there is still a possibility that the impact on CA1 pyramidal cell excitability could affect their response to incoming inputs. We think that the second component, that is, alterations of OLM and PV IN modulation of pyramidal cell inputs, is the most likely.

Another critical CA1 hippocampal function is the ability to organize cellular activity representing episodes of few seconds into individual θ cycles. While computational models suggest that IN function is critical for such sequence organization (Cutsuridis and Hasselmo 2012; Hasselmo and Stern 2014; Chadwick et al. 2015), it has never been demonstrated in vivo. To investigate this phenomenon, we examined pairwise correlations between place cells with overlapping fields. As others (Skaggs et al. 1996; Dragoi and Buzsáki 2006) have showed, we found that there was a significant correlation between the distance separating the peaks of pairs of cells with overlapping fields and the spiking interval between the cells within θ cycles. Including large interfield distances, this relationship was taking the shape of a sigmoid. Under Nav1.1 KD, this sigmoid was shorter and reached its asymptote earlier. This suggests that distance was poorly represented within θ cycles and that the maximal distance to be represented was shorter. Importantly, there was no difference in terms of θ frequency and power between groups. Rather, theta modulation of CCGs decreased significantly. Therefore, we conclude that it is the coordination of pyramidal cell discharges with regard to θ, that is, the pyramidal cell phase shift, that influences the sigmoid shape, rather than θ itself being altered in the Nav1.1 KD group.

Behavioral Consequences of Focal Nav1.1 KD

Overall, electrophysiological changes show that place cell spatial precision and temporal organization are altered by Nav1.1 KD resulting in degraded spatial and distance representations. However, those representations persist since place cells are present in our Nav1.1 KD group and they still show θ phase precession and θ compression, albeit degraded. Furthermore, the viral infection was contained unilaterally in the right dorsal hippocampus of adult rats. Nav1.1 KD rats showed behavioral impairment in the spatial component of the novelty recognition task. Interestingly, this impairment cannot be interpreted as a total forgetting of spatial information based on the inability to notice the object location change but rather as a more subtle effect where Nav1.1 KD rats persisted in exploring the previous location of the moved object. This is in line with previous studies showing that, unlike CA3 or global hippocampal lesions, neither dorsal- nor ventral-selective CA1 lesion altered the performance in a novelty recognition task in rats (regardless of the nature of the change: odor, spatial, or visual). Unfortunately, we cannot compare our results further, as those studies do not take into account the exploration of the previous location of the moved object. Nevertheless, others have shown that CA1 lesioned rats were impaired in temporal ordering tasks emphasizing the importance of CA1 for the temporal organization of spatial information (Hoge and Kesner 2007). It is tempting to conclude that our behavioral result confirms a place/distance representation alteration by Nav1.1 KD as suggested by our θ phase compression data.

However, one cannot exclude that some of the behavioral changes observed also result from the impact of these local network alterations on long-range connectivity and on the function of other circuits. For instance, although the change in θ phase precession and place cell dynamics is indeed expected to contribute to spatial learning deficits, the local manipulations in the dorsal hippocampus could also affect other brain states (i.e., perturb sleep-wake cycles, altered sleep-related memory consolidation (Khodagholy et al. 2017) that, in turn, may also contribute to the spatial learning impairments.

Conclusion and Significance Regarding Neurological Disorders

In this study, Nav1.1 KD is not intended to be a model of any specific neurological disorder. In DS, genetic alterations impair Nav1.1 function in the whole brain and throughout development. In AD, amyloid beta and phosphorylated tau accumulate in many brain areas leading to a multitude of physiologic effects (one of which has been shown to be reduced sodium channel expression) and ultimately neuronal death. In contrast, here, we have selectively altered Nav1.1 expression in the dorsal hippocampus in adult rats. This approach has allowed us to evaluate formally how Nav1.1 knockdown leads to a microcircuit disruption in a brain structure that is critically important for spatial cognition and, therefore, better understand its normal function in such networks. By extension, our results demonstrate that the function of Nav1.1 is essential for the integrity of such networks and imply that the loss of function could similarly affect these networks in disease models.

Overall, our study shows that local KD of Nav1.1 in CA1 is sufficient to impair IN excitability and the temporal organization of their firing with regard to theta oscillations. The consequence of this impaired inhibition is a dysregulation of CA1 microcircuits leading to an alteration of place cell temporal coordination and impaired spatial memory. In a snowball-like effect, one can imagine that such temporal discoordination may prevent the optimal integration of place cell signal in downstream structures such as the subiculum (Kim et al. 2012). Such a scenario, amplified in the context of more regional Nav1.1 alterations (such as in the hippocampal down-regulation observed in AD) or in a whole brain *SCN1A* mutation (such as in DS or ASD), could explain the catastrophic behavioral and cognitive phenotypes observed in Nav1.1-related neurological syndromes.

While our results suggest a direct effect of Nav1.1 KD on network function and behavior, caution should be taken not to misinterpret these results and consider that, in terms of DS, for example, the impact of other factors, such as seizures, is not important. To the contrary, we have proposed that both seizures and the sodium channel function are relevant for cognitive impairment and that their effects may be multiplicative. In a recent study, Salgueiro-Pereira et al. (Salgueiro-Pereira et al. 2019) induced, at the age of disease onset, a series of short

seizures in mice carrying a *Scn1a* mutation with a mild/asymptomatic phenotype. Seizure-exposed *Scn1a* mice, but not controls, developed severe DS-like phenotypes, such as spontaneous seizures and cognitive impairment. Therefore, seizures occurring in a context of a mutation can have multiplying effects on cognitive impairment. Nevertheless, the results of our current and past studies (Bender et al. 2013, 2016) show that Nav1.1 KD has a direct effect on network function. Therefore, treatments focusing on neuronal coordination in addition to seizure suppression may be beneficial. As an illustration, Han et al. (2012) showed that enhancing GABA-mediated signaling (with clonazepam) in *Scn1a* +/− mice rescued autistic-like behaviors and cognitive comorbidities, demonstrating that these deficits are at least in part due to reduced GABAergic tone.

Overall, our results highlight the direct role of Nav1.1 in IN fast spiking activity and the impact their dysregulation can have at the network and behavioral levels. By extension, our study provides support for the neuronal coordination hypothesis and highlights the critical role of INs in this process. We propose that similar mechanisms, characterized by alterations of the neuronal syntax (Buzsáki and Watson 2012; Barry et al. 2016), are at play in several neurological and psychiatric disorders and may explain the phenotypic overlap between them.

Supplementary Material

Supplementary material can be found at *Cerebral Cortex* online.

Funding

A grant from the National Institutes of Health to P.P.L.S. (R01NS076763).

Notes

We would like to thank Drs Amanda Hernan and Federica Bertaso for reading the manuscript and giving valuable feedback.
Conflict of Interest: None.

Authors Contribution

S.S., R.S., and P.P.L.S. developed the concept of this study; S.S. and P.P.L.S. designed the experiments. A.C.B. designed the shRNA construct and produced the lentivirus. S.S. acquired data. S.S., S.B., R.S., and P.P.L.S. analyzed data. S.S. and P.P.L.S. wrote the manuscript and designed figures.

References

Acsády L, Görcs TJ, Freund TF. 1996. Different populations of vasoactive intestinal polypeptide-immunoreactive interneurons are specialized to control pyramidal cells or interneurons in the hippocampus. *Neuroscience*. 73:317–334.

Amemiya S, Redish AD. 2018. Hippocampal theta-gamma coupling reflects state-dependent information processing in decision making. *Cell Rep*. 22:3328–3338.

Barry JM, Sakkaki S, Barriere SJ, Patterson KP, Lenck-Santini PP, Scott RC, Baram TZ, Holmes GL. 2016. Temporal coordination of hippocampal neurons reflects cognitive outcome post-febrile status epilepticus. *EBioMedicine*. 7:175–190.

Barthó P, Hirase H, Monconduit L, Zugaro M, Harris KD, Buzsáki G, Bartho P, Hirase H, Monconduit L, Zugaro M *et al*. 2004. Characterization of neocortical principal cells and interneurons by network interactions and extracellular features. *J Neurophysiol*. 92:600–608.

Bender AC, Luikart BW, Lenck-Santini P-P, Barth A, Cobos I, Ho K. 2016. Cognitive deficits associated with Nav1.1 alterations: involvement of neuronal firing dynamics and oscillations. *PLoS one*. 11:e0151538.

Bender AC, Natola H, Ndong C, Holmes GL, Scott RC, Lenck-Santini P-P. 2013. Focal Scn1a knockdown induces cognitive impairment without seizures. *Neurobiol Dis*. 54:297–307.

Bieri KW, Bobbitt KN, Colgin LL. 2014. Slow and fast gamma rhythms coordinate different spatial coding modes in hippocampal place cells. *Neuron*. 82:670–681.

Buzsáki G. 2002. Theta oscillations in the hippocampus. *Neuron*. 33:325–340.

Buzsáki G. 2010. Neural syntax: cell assemblies, synapsembles, and readers. *Neuron*. 68:362–385.

Buzsáki G, Wang X-J. 2012. Mechanisms of gamma oscillations. *Annu Rev Neurosci*. 35:203–225.

Buzsáki G, Watson BO. 2012. Brain rhythms and neural syntax: implications for efficient coding of cognitive content and neuropsychiatric disease. *Dialogues Clin Neurosci*. 14:345–367.

Catterall WA, Kalume F, Oakley JC. 2010. NaV1.1 channels and epilepsy. *J Physiol*. 588:1849–1859.

Chadwick A, Van Rossum MCW, Nolan MF. 2015. Independent theta phase coding accounts for ca population sequences and enables flexible remapping. *Elife*. 2015:1–51.

Cheah CS, Yu FH, Westenbroek RE, Kalume FK, Oakley JC, Potter GB, Rubenstein JL, Catterall WA. 2012. Specific deletion of NaV1.1 sodium channels in inhibitory interneurons causes seizures and premature death in a mouse model of Dravet syndrome. *Proc Natl Acad Sci*. 109:14646–14651.

Craig MT, McBain CJ. 2015. Fast gamma oscillations are generated intrinsically in CA1 without the involvement of fast-spiking basket cells. *J Neurosci*. 35:3616–3624.

Cutsuridis V, Hasselmo M. 2012. GABAergic contributions to gating, timing, and phase precession of hippocampal neuronal activity during theta oscillations. *Hippocampus*. 22:1597–1621.

Czurkó A, Huxter J, Li Y, Hangya B, Muller RU. 2011. Theta phase classification of interneurons in the hippocampal formation of freely moving rats. *J Neurosci*. 31:2938–2947.

D'Gama AM, Pochareddy S, Li M, Jamuar SS, Reiff RE, Lam A-TN, Sestan N, Walsh CA. 2015. Targeted DNA sequencing from autism spectrum disorder brains implicates multiple genetic mechanisms. *Neuron*. 88:910–917.

Dragoi G, Buzsáki G. 2006. Temporal encoding of place sequences by hippocampal cell assemblies. *Neuron*. 50:145–157.

Dutton SB, Makinson CD, Papale LA, Shankar A, Balakrishnan B, Nakazawa K, Escayg A. 2013. Preferential inactivation of Scn1a in parvalbumin interneurons increases seizure susceptibility. *Neurobiol Dis*. 49:211–220.

Feng T, Silva D, Foster DJ. 2015. Dissociation between the experience-dependent development of hippocampal theta sequences and single-trial phase precession. *J Neurosci*. 35:4890–4902.

Fenton AA. 2015. Excitation-inhibition discoordination in rodent models of mental disorders. *Biol Psychiatry*. 77:1079–1088.

Fernández-Ruiz A, Oliva A, Nagy GA, Maurer AP, Berényi A, Buzsáki G. 2017. Entorhinal-CA3 dual-input control of spike timing in the hippocampus by theta-gamma coupling. *Neuron*. 93: 1213–1226.e5.

Fisher NI. 1993. *Statistical Analysis of Circular Data*, Cambridge, UK: Cambridge University Press.

Grienberger C, Milstein AD, Bittner KC, Romani S, Magee JC. 2017. Inhibitory suppression of heterogeneously tuned excitation enhances spatial coding in CA1 place cells. *Nat Neurosci*. 20:417–426.

Han S, Tai C, Westenbroek RE, Yu FH, Cheah CS, Potter GB, Rubenstein JL, Scheuer T, de la Iglesia HO, Catterall WA. 2012. Autistic-like behaviour in Scn1a+/− mice and rescue by enhanced GABA-mediated neurotransmission. *Nature*. 489:385–390.

Hasselmo ME, Stern CE. 2014. Theta rhythm and the encoding and retrieval of space and time. *Neuroimage*. 85:656–666.

Higurashi N, Uchida T, Lossin C, Misumi Y, Okada Y, Akamatsu W, Imaizumi Y, Zhang B, Nabeshima K, Mori XM *et al*. 2013. A human Dravet syndrome model from patient induced pluripotent stem cells. *Mol Brain*. 22:4241–4252.

Hoge J, Kesner RP. 2007. Role of CA1 and CA3 subregions of the dorsal hippocampus on temporal processing of objects. *Neurobiology of Learning and Memory* 88:225–231.

Inostroza M, Brotons-Mas JR, Laurent F, Cid E, de la Prida LM. 2013. Specific impairment of "what-where-when" episodic-like memory in experimental models of temporal lobe epilepsy. *J Neurosci*. 33:17749–17762.

Jensen HS, Grunnet M, Bastlund JF. 2014. Therapeutic potential of NaV1.1 activators. *Trends Pharmacol Sci*. 35:113–118.

Khodagholy D, Gelinas JN, Buzsáki G. 2017. Learning-enhanced coupling between ripple oscillations in association cortices and hippocampus. *Science*. 358:369–372.

Kim SM, Ganguli S, Frank LM. 2012. Spatial information outflow from the hippocampal circuit: distributed spatial coding and phase precession in the subiculum. *J Neurosci*. 32:11539–11558.

Klausberger T, Somogyi P. 2008. Neuronal diversity and temporal dynamics: the unity of hippocampal circuit operations. *Science*. 321:53–57.

Lasztóczi B, Klausberger T. 2014. Layer-specific GABAergic control of distinct gamma oscillations in the CA1 hippocampus. *Neuron*. 81:1126–1139.

Lenck-Santini P-P, Holmes GL. 2008. Altered phase precession and compression of temporal sequences by place cells in epileptic rats. *J Neurosci*. 28:5053–5062.

Lenck-Santini P, Save E, Poucet B. 2001. Evidence for a relationship between place-cell spatial firing and spatial memory performance. *Hippocampus*. 11:377–390.

Lisman J, Redish AD. 2009. Prediction, sequences and the hippocampus. *Philos Trans R Soc Lond B Biol Sci*. 364:1193–1201.

Liu Y, Lopez-Santiago LF, Yuan Y, Jones JM, Zhang H, O'Malley HA, Patino GA, O'Brien JE, Rusconi R, Gupta A *et al*. 2013. Dravet syndrome patient-derived neurons suggest a novel epilepsy mechanism. *Ann Neurol*. 74:128–139.

Lopez-Pigozzi D, Laurent F, Brotons-Mas JR, Valderrama M, Valero M, Fernandez-Lamo I, Cid E, Gomez-Dominguez D, Gall B, de la Prida LM. 2016. Altered oscillatory dynamics of CA1 parvalbumin basket cells during theta-gamma rhythmopathies of temporal lobe epilepsy. *eNeuro*. 3:1–20.

Lovett-Barron M, Turi GF, Kaifosh P, Lee PH, Bolze F, Sun X-H, Nicoud J-F, Zemelman BV, Sternson SM, Losonczy A. 2012. Regulation of neuronal input transformations by tunable dendritic inhibition. *Nat Neurosci*. 15:423–430.

Mahoney K, Moore SJ, Buckley D, Alam M, Parfrey P, Penney S, Merner N, Hodgkinson K, Young T-L. 2009. Variable neurologic phenotype in a GEFS+ family with a novel mutation in SCN1A. *Seizure*. 18:492–497.

Mann EO, Radcliffe CA, Paulsen O. 2005. Hippocampal gamma-frequency oscillations: from interneurones to pyramidal cells, and back. *J Physiol*. 562:55–63.

Martinez-Losa M, Tracy TE, Ma K, Verret L, Clemente-Perez A, Khan AS, Cobos I, Ho K, Gan L, Mucke L *et al*. 2018. Nav1.1-overexpressing interneuron transplants restore brain rhythms and cognition in a mouse model of Alzheimer's disease. *Neuron*. 98: 75–89.e5.

Maurer AP, Cowen SL, Burke SN, Barnes CA, McNaughton BL. 2006. Phase precession in hippocampal interneurons showing strong functional coupling to individual pyramidal cells. *J Neurosci*. 26:13485–13492.

Mehta MR, Lee AK, Wilson MA. 2002. Role of experience and oscillations in transforming a rate code into a temporal code. *Nature*. 417:741–746.

Mizuseki K, Sirota A, Pastalkova E, Buzsáki G. 2009. Theta oscillations provide temporal windows for local circuit computation in the entorhinal-hippocampal loop. *Neuron*. 64: 267–280.

Muller RU, Kubie JL, Ranck JB. 1987. Spatial firing patterns of hippocampal complex-spike cells in a fixed environment. *J Neurosci*. 7:1935–1950.

Nabbout R, Chemaly N, Chipaux M, Barcia G, Bouis C, Dubouch C, Leunen D, Jambaqué I, Dulac O, Dellatolas G *et al*. 2013. Encephalopathy in children with Dravet syndrome is not a pure consequence of epilepsy. *Orphanet J Rare Dis*. 8:176.

O'Keefe J, Recce ML. 1993. Phase relationship between hippocampal place units and the EEG theta rhythm. *Hippocampus*. 3:317–330.

Ogiwara I, Miyamoto H, Morita N, Atapour N, Mazaki E, Inoue I, Takeuchi T, Itohara S, Yanagawa Y, Obata K *et al*. 2007. Nav1.1 localizes to axons of parvalbumin-positive inhibitory interneurons: a circuit basis for epileptic seizures in mice carrying an Scn1a gene mutation. *J Neurosci*. 27:5903–5914.

Passamonti C, Petrelli C, Mei D, Foschi N, Guerrini R, Provinciali L, Zamponi N. 2015. A novel inherited SCN1A mutation associated with different neuropsychological phenotypes: is there a common core deficit? *Epilepsy & Behavior*. 43:89–92.

Paxinos G, Watson C. 2007. *The rat brain in stereotaxic coordinates*. Academic Press: Cambridge MS USA.

Richard GR, Titiz A, Tyler A, Holmes GL, Scott RC, Lenck-Santini P. 2013. Speed modulation of hippocampal theta frequency correlates with spatial memory performance. *Hippocampus*. 23:1269–1279.

Robbe D, Buzsáki G. 2009. Alteration of theta timescale dynamics of hippocampal place cells by a cannabinoid is associated with memory impairment. *J Neurosci*. 29:12597–12605.

Royer S, Zemelman BV, Losonczy A, Kim J, Chance F, Magee JC, Buzsáki G, Buzsaki G. 2012. Control of timing, rate and bursts of hippocampal place cells by dendritic and somatic inhibition. *Nat Neurosci*. 15:769–775.

Salgueiro-Pereira AR, Duprat F, Pousinha PA, Loucif A, Douchamps V, Regondi C, Ayrault M, Eugie M, Stunault MI, Escayg A *et al*. 2019. A two-hit story: seizures and genetic mutation interaction sets phenotype severity in SCN1A epilepsies. *Neurobiol Dis*. 125:31–44.

Schmidt R, Diba K, Leibold C, Schmitz D, Buzsáki G, Kempter R. 2009. Single-trial phase precession in the hippocampus. *J Neurosci*. 29:13232–13241.

Senior TJ, Huxter JR, Allen K, O'Neill J, Csicsvari J. 2008. Gamma oscillatory firing reveals distinct populations of pyramidal

cells in the CA1 region of the hippocampus. *J Neurosci*. 28:2274–2286.

Skaggs WE, McNaughton BL, Wilson MA, Barnes CA, Skaggs BL, Wilson MA, Barnes CA. 1996. Theta phase precession in hippocampal neuronal populations and the compression of temporal sequences. *Hippocampus*. 6:149–172.

Stark E, Eichler R, Roux L, Fujisawa S, Rotstein HG, Buzsáki G. 2013. Inhibition-induced theta resonance in cortical circuits. *Neuron*. 80:1263–1276.

Tai C, Abe Y, Westenbroek RE, Scheuer T, Catterall WA. 2014. Impaired excitability of somatostatin- and parvalbumin-expressing cortical interneurons in a mouse model of Dravet syndrome. *Proc Natl Acad Sci*. 111:3139–3148.

Tsodyks MV, Skaggs WE, Sejnowski TJ, McNaughton BL. 1997. Paradoxical effects of external modulation of inhibitory interneurons. *J Neurosci*. 17:4382–4388.

Uhlhaas PJ, Singer W. 2010. Abnormal neural oscillations and synchrony in schizophrenia. *Nat Rev Neurosci*. 11:100–113.

Verret L, Mann EO, Hang GB, Barth AM, Cobos I, Ho K, Devidze N, Masliah E, Kreitzer AC, Mody I *et al*. 2012. Inhibitory interneuron deficit links altered network activity and cognitive dysfunction in Alzheimer model. *Cell*. 149: 708–721.

Vertes RP, Hoover WB, Viana Di Prisco G. 2004. Theta rhythm of the hippocampus: subcortical control and functional significance. *Behav Cogn Neurosci Rev*. 3: 173–200.

Villeneuve N, Laguitton V, Viellard M, Lépine A, Chabrol B, Dravet C, Milh M. 2014. Cognitive and adaptive evaluation of 21 consecutive patients with Dravet syndrome. *Epilepsy Behav*. 31:143–148.

Yu FH, Mantegazza M, Westenbroek RE, Robbins CA, Kalume F, Burton KA, Spain WJ, McKnight GS, Scheuer T, Catterall WA. 2006. Reduced sodium current in GABAergic interneurons in a mouse model of severe myoclonic epilepsy in infancy. *Nat Neurosci*. 9:1142–1149.